Int. J. Solids Structures Vol. 30, No. 16, pp. 2163–2175, 1993
Printed in Great Britain

0020-7683/93 $6.00+ .00

THE STRESS INTENSITY FACTOR OF A SUBSURFACE INCLINED CRACK SUBJECTED TO DYNAMIC IMPACT LOADING

CHWAN-HUEI TSAI
Department of Mechanical Engineering, Huafan Institute of Technology, Taipei Hsien, Taiwan 223, Republic of China

and

CHIEN-CHING MA
Department of Mechanical Engineering, National Taiwan University, No. 1 Roosevelt Rd., Sec. 4, Taipei, Taiwan 10764, Republic of China

(*Received* 8 *November* 1992 ; *in revised form* 3 *March* 1993)

Abstract—To gain insight into the phenomenon of the interaction of stress waves with a material defect, the transient problem of a half-space containing a subsurface inclined semi-infinite crack subjected to normal impact on the boundary of the half-space is studied. The solutions are determined by linear superposition of the fundamental solution in the Laplace transform domain. The fundamental solution is the exponentially distributed traction on crack faces proposed by Tsai and Ma (1992, *J. Appl. Mech.* **59**, 804–811). Due to the nature of the crack geometry, a combination of transient mixed mode I and II deformation fields is induced near the crack tip. The exact closed form solutions of stress intensity factor histories are obtained. These solutions are valid for the time interval from initial loading until the first wave scattered at the crack tip returns to the crack tip after being reflected by the free boundary. The probable crack propagation direction is predicted from different fracture criteria.

1. INTRODUCTION

The difficulty in determining the transient stress field in a crack-elastic body subjected to dynamic loading is well known. The investigation of an idealized semi-infinite crack can provide some information for a realistic elastodynamic fracture problem. It is noted that while the analysis has been carried out assuming a semi-infinite crack, the results remain valid for a finite crack up until the time at which waves diffracted from the far tip reach the tip near the boundary. The incident wave generated by the normal impact on the half-space will be reflected from the crack surfaces and diffracted by the crack tip. The stress intensity factors vary rapidly at the instant a wave front passes through the crack tip. The value of the peak is often greater than the corresponding static value and might induce brittle fracture. The failure of a notched beam due to impact, called the dynamic tear test, was studied by Brock *et al.* (1985). They investigated the case in which the crack is normal to the half-plane surface and the point load is applied to the surface directly above the crack tip.

In conventional studies of a semi-infinite crack in an unbounded medium subjected to dynamic loading, the complete solution is obtained by integral transform methods together with direct application of the Wiener–Hopf technique (Noble, 1958) and the Cagniard–de Hoop method (de Hoop, 1958) of Laplace inversion. If the loading is replaced by a nonuniform distribution having a characteristic length, then the same procedure using integral transformation methods does not apply. Freund (1974) studied the problem of an elastic solid containing a half-plane crack subjected to concentrated impact loading on the faces of the crack. He proposed a fundamental solution arising from an edge dislocation climbing along the positive x_1 axis with a constant speed to overcome the difficulties of the case with characteristic length. The solution can be constructed by taking an integration over a climbing dislocation of different velocity. Basing their procedures on this method, Brock (1982, 1984), Brock *et al.* (1985) and Ma and Hou (1990, 1991) analysed a series of problems of a semi-infinite crack subjected to impact loading. Recently, Lee and Freund

(1990) analysed fracture initiation of an edge cracked plate subjected to an asymmetric impact.

The problem to be considered in this study is the plane strain response of an elastic half-plane, with an inclined crack extending from infinity to the half-plane surface, subjected to a dynamic impact loading on its surface. Particular attention is given to the elastic field near the crack tip, which is completely characterized by the stress intensity factor. This problem involves a characteristic length which makes a direct solution by standard techniques difficult. Furthermore, none of the methods proposed by Freund (1974) and Brock *et al.* (1985) work for this problem. Therefore, some other approach must be followed. A new fundamental solution proposed by Tsai and Ma (1992) is used to overcome these difficulties. This alternative fundamental solution is successfully applied to solve the problem and will be demonstrated to be an efficient methodology. The final formulations are expressed explicitly and the dynamic effect of each wave is presented in a closed form. The results are valid before the first wave scatttered from crack tip returns to the crack tip after being reflected by the free boundary. By setting time frames properly, we drop the interaction of the crack surface and the half space. The half space effects on loadings are still included. The investigation of the dynamic tear test by Brock *et al.* (1985) will be a special case of the general formulation in this study. A realistic impact loading, with a rise time, effecting a uniform distributed traction on the half-plane surface is also analysed in present work. Finally, two fracture criteria, those of maximum circumferential tensile stress proposed by Erdogan and Sih (1963) and minimum strain energy density proposed by Sih (1972), are used to determine the possible direction of crack propagation.

2. FUNDAMENTAL SOLUTIONS

As usual in problems of the type considered here, superposition of solutions plays a significant role. The solutions to the problems considered in this study can be determined by superposition of the following problems A and B. Problem A treats the dynamic force acting on the same semi-infinite half-plane without a crack, inducing a traction on the planes that will eventually define the initial crack faces. In problem B, an infinite body containing a semi-infinite crack is considered in which the faces are subjected to tractions which are equal and opposite to those on the corresponding planes in problem A. The sum of the solutions to problems A and B is the solution to the problem of diffraction of incident waves by a stationary inclined crack.

From physical considerations, reflected and diffracted fields are generated to eliminate the stress induced by incident waves on the traction-free boundaries of crack faces. For most of the dynamic problems, the incident waves can be represented in an exponential functional form in the Laplace transform domain of time. Unlike usual superposition methods which are performed in the time domain, the superposition scheme proposed in this study is performed in the Laplace transform domain. This methodology allows us to solve more general and difficult problems.

Consider plane strain deformation of a semi-infinite crack contained in an unbounded medium. An exponentially distributed traction in the Laplace transform domain is applied to the crack faces. The traction force can be divided into a normal force (mode I) and a tangential force (mode II). Because of the symmetry with respect to the plane $x_2 = 0$, the problem can be viewed as a half-plane problem with the material occupying the region $x_2 \geqslant 0$, subject to the boundary conditions

$$\begin{aligned} \bar{\sigma}_{22}(x_1, 0, p) &= e^{pdx_1}, \quad -\infty < x_1 \leqslant 0, \\ \bar{\sigma}_{12}(x_1, 0, p) &= 0, \quad -\infty < x_1 < \infty, \\ \bar{u}_2(x_1, 0, p) &= 0, \quad 0 \leqslant x_1 < \infty \end{aligned} \tag{1}$$

for mode I and

$$\bar{\sigma}_{22}(x_1, 0, p) = 0, \qquad -\infty < x_1 < \infty,$$
$$\bar{\sigma}_{12}(x_1, 0, p) = e^{pdx_1}, \qquad -\infty < x_1 \leqslant 0,$$
$$\bar{u}_1(x_1, 0, p) = 0, \qquad 0 \leqslant x_1 < \infty \tag{2}$$

for mode II, where p is the Laplace transform parameter and d is a constant. The overbar symbol is used to denote the transform on time t. The final results of the dynamic mode I and mode II stress intensity factors in the Laplace transform domain are

$$\bar{K}_I(p) = -\sqrt{\frac{2}{p}} K_I^F(d), \quad \bar{K}_{II}(p) = -\sqrt{\frac{2}{p}} K_{II}^F(d), \tag{3}$$

where

$$K_I^F(d) = \frac{(a+d)^{1/2}}{(c+d)S_+(d)}, \quad K_{II}^F(d) = \frac{(b+d)^{1/2}}{(c+d)S_+(d)},$$
$$S_+(d) = \exp\left(\frac{-1}{\pi}\int_a^b \tan^{-1}\left[\frac{4\lambda^2(\lambda^2-a^2)^{1/2}(b^2-\lambda^2)^{1/2}}{(b^2-2\lambda^2)^2}\right]\frac{d\lambda}{\lambda+d}\right),$$

$a = \sqrt{\rho/(\gamma+2\mu)}$, $b = \sqrt{\rho/\mu}$, a, b and c are the slownesses of the longitudinal wave, shear wave and Rayleigh wave, μ and ρ and shear modulus and mass density, and γ the Lamé elastic constant.

3. SUBSURFACE CRACK DUE TO SURFACE IMPACT

The investigation of a subsurface crack subjected to dynamic loading is an important topic in material failure analysis. The failure of a notched beam induced by impact loading is often used to study the dynamic fracture of material. In the time period during which waves generated by the impact force and its diffractions at the notch end have not returned to the crack tip, the problem for the determination of the dynamic stress intensity factor can be treated as a semi-infinite crack contained in an unbounded medium. The problem considered here is an inclined semi-infinite crack located under the surface of a half-plane as shown in Fig. 1(a). The origins of the two coordinate systems $(\bar{x}_1, \bar{x}_2)$ and (x_1, x_2) are

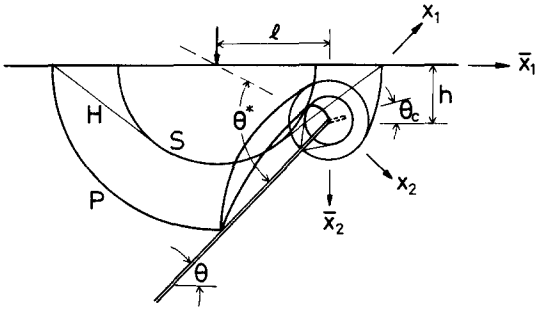

Fig. 1(a). Configuration, coordinate system and wave fronts of a subsurface crack subjected to concentrated impact loading.

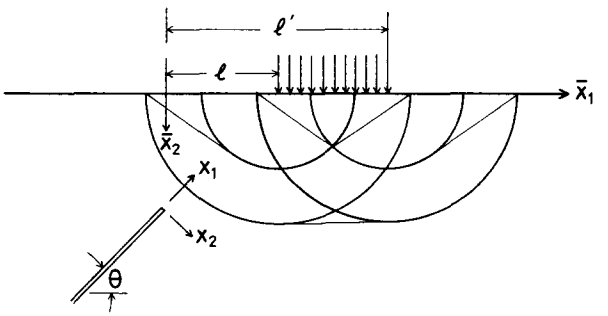

Fig. 1(b). Wave fronts of a subsurface crack subjected to uniformly distributed impact loading.

located at the plane surface and crack tip, respectively. The planar crack lies in the plane $x_2 = 0, x_1 < 0$ and the inclined angle of the crack is θ. The coordinate transforms and stress relations between these two systems are

$$\begin{aligned} \bar{x}_1 &= x_1 \cos\theta + x_2 \sin\theta, \\ \bar{x}_2 &= -x_1 \sin\theta + x_2 \cos\theta + h, \end{aligned} \tag{4}$$

$$\begin{aligned} \sigma_{22} &= \sigma_{\bar{1}\bar{1}} \sin^2\theta + \sigma_{\bar{2}\bar{2}} \cos^2\theta + \sigma_{\bar{1}\bar{2}} \sin 2\theta, \\ \sigma_{12} &= \tfrac{1}{2}(\sigma_{\bar{1}\bar{1}} - \sigma_{\bar{2}\bar{2}}) \sin 2\theta + \sigma_{\bar{1}\bar{2}} \cos 2\theta, \end{aligned} \tag{5}$$

where h is the vertical distance from the crack tip to the plane surface.

A concentrated point impact loading of Heaviside function $H(t)$ time dependence is applied at the position $\bar{x}_1 = l$ at time $t = 0$. The corresponding stress intensity factor histories are determined exactly by linear superposition of the two readily obtainable stress wave propagation solutions. One is Lamb's problem (1904) of an applied point loading on the surface with no crack. The other problem is a semi-infinite crack in an unbounded medium whose surfaces are subjected to the negatives of stresses induced on the region that would be occupied by the crack in Lamb's problem. But only the latter part will induce the singular stress in the crack tip. The stress intensity factor histories obtained in this study are valid for the time interval from initial loading to the return of the first wave scattered at the crack tip to the crack tip after reflection from the plane surface. The solutions to Lamb's problem in Laplace transform form are

$$\bar{\sigma}_{22}(\bar{x}_1, \bar{x}_2, p) = \frac{1}{2\pi i} \int_B A_1(\lambda)\, e^{-p\alpha\bar{x}_2 + p\lambda(\bar{x}_1 - l)} + A_2(\lambda)\, e^{-p\beta\bar{x}_2 + p\lambda(\bar{x}_1 - l)}\, d\lambda, \tag{6}$$

$$\bar{\sigma}_{12}(\bar{x}_1, \bar{x}_2, p) = \frac{1}{2\pi i} \int_B A_3(\lambda)\, e^{-p\alpha\bar{x}_2 + p\lambda(\bar{x}_1 - l)} + A_4(\lambda)\, e^{-p\beta\bar{x}_2 + p\lambda(\bar{x}_1 - l)}\, d\lambda, \tag{7}$$

where B is the usual inversion path for the two-sided Laplace transform from $\lambda_1 - i\infty$ to $\lambda_1 + i\infty$, and λ_1 is a real number located in the interval $|\lambda_1| < a$. The functions in (6) and (7) are

$$\begin{aligned} A_1(\lambda) &= -\frac{(b^2 - 2\lambda^2)^2}{R} \cos^2\theta - \frac{(b^2 - 2\alpha^2)(b^2 - 2\lambda^2)}{R} \sin^2\theta + \frac{2\alpha\lambda(b^2 - 2\lambda^2)}{R} \sin 2\theta, \\ A_2(\lambda) &= \frac{4\alpha\beta\lambda^2}{R} \sin^2\theta - \frac{4\alpha\beta\lambda^2}{R} \cos^2\theta - \frac{2\alpha\lambda(b^2 - 2\lambda^2)}{R} \sin 2\theta, \\ A_3(\lambda) &= \frac{(b^2 - 2\lambda^2)(a^2 - 2\lambda^2)}{R} \sin 2\theta + \frac{2\alpha\lambda(b^2 - 2\lambda^2)}{R} \cos 2\theta, \\ A_4(\lambda) &= \frac{4\alpha\beta\lambda^2}{R} \sin 2\theta - \frac{2\alpha\lambda(b^2 - 2\lambda^2)}{R} \cos 2\theta, \\ \alpha &= \sqrt{a^2 - \lambda^2}, \quad \beta = \sqrt{b^2 - \lambda^2}, \quad R = (b^2 - 2\lambda^2)^2 + 4\alpha\beta\lambda^2. \end{aligned} \tag{8}$$

The stresses in the crack surfaces induced by the incident waves of Lamb's problem

can be obtained from (6) and (7) by taking the coordinate transform and letting $x_2 = 0$, so that

$$\bar{\sigma}_{22} = \frac{1}{2\pi i}\int_B A_1(\lambda)\,e^{p(\lambda\cos\theta+\alpha\sin\theta)x_1-p\alpha h-p\lambda l} + A_2(\lambda)\,e^{p(\lambda\cos\theta+\beta\sin\theta)x_1-p\beta h-p\lambda l}\,d\lambda, \tag{9}$$

$$\bar{\sigma}_{12} = \frac{1}{2\pi i}\int_B A_3(\lambda)\,e^{p(\lambda\cos\theta+\alpha\sin\theta)x_1-p\alpha h-p\lambda l} + A_4(\lambda)\,e^{p(\lambda\cos\theta+\beta\sin\theta)x_1-p\beta h-p\lambda l}\,d\lambda. \tag{10}$$

It is shown that tractions in crack surfaces are represented by the exponential functions $e^{p(\lambda\cos\theta+\alpha\sin\theta)x_1}$ and $e^{p(\lambda\cos\theta+\beta\sin\theta)x_1}$. Since the stress intensity factors resulting from applied tractions e^{pdx_1} are expressed in (3), the solution of this problem can be constructed by superposition of the fundamental solution obtained in the previous section. Replacing d with $\lambda\cos\theta+\alpha\sin\theta$ and $\lambda\cos\theta+\beta\sin\theta$ and combining (3), (9) and (10), the results for the mixed mode dynamic stress intensity factors in the Laplace transform domain can be expressed as

$$\bar{K}_{\mathrm{I}} = \frac{1}{\sqrt{2p\pi i}}\int_B A_1(\lambda)K_{\mathrm{I}}^{\mathrm{F}}(\lambda\cos\theta+\alpha\sin\theta)\,e^{-p\alpha h-pyl} + A_2(\lambda)K_{\mathrm{I}}^{\mathrm{F}}(\lambda\cos\theta+\beta\sin\theta)\,e^{-p\beta h-p\lambda l}\,d\lambda, \tag{11}$$

$$\bar{K}_{\mathrm{II}} = \frac{1}{\sqrt{2p\pi i}}\int_B A_3(\lambda)(K_{\mathrm{II}}^{\mathrm{F}}\lambda\cos\theta+\alpha\sin\theta)\,e^{-p\alpha h-p\lambda l} + A_4(\lambda)K_{\mathrm{II}}^{\mathrm{F}}(\lambda\cos\theta+\beta\sin\theta)\,e^{-p\beta h-p\lambda l}\,d\lambda. \tag{12}$$

Finally, the mixed mode stress intensity factors in the time domain can be obtained by employing Cagniard's method:

$$\frac{\pi^{3/2}}{\sqrt{2}}K_{\mathrm{I}}(t) = \int_{ar_0}^{t}\frac{1}{\sqrt{t-\tau}}\,\mathrm{Im}\left[A_1(\lambda_1)K_{\mathrm{I}}^{\mathrm{F}}(\lambda_1\cos\theta+\alpha\sin\theta)\frac{\partial\lambda_1}{\partial\tau}\right]d\tau + \int_{T_{H_0}}^{t}\frac{1}{\sqrt{t-\tau}}\,\mathrm{Im}\left[A_2(\lambda_2)K_{\mathrm{I}}^{\mathrm{F}}(\lambda_2\cos\theta+\beta\sin\theta)\frac{\partial\lambda_2}{\partial\tau}\right]H(br_0-\tau)\,d\tau + \int_{br_0}^{t}\frac{1}{\sqrt{t-\tau}}\,\mathrm{Im}\left[A_2(\lambda_3)K_{\mathrm{I}}^{\mathrm{F}}(\lambda_3\cos\theta+\beta\sin\theta)\frac{\partial\lambda_3}{\partial\tau}\right]d\tau, \tag{13}$$

$$\frac{\pi^{3/2}}{\sqrt{2}}K_{\mathrm{II}}(t) = \int_{ar_0}^{t}\frac{1}{\sqrt{t-\tau}}\,\mathrm{Im}\left[A_3(\lambda_1)K_{\mathrm{II}}^{\mathrm{F}}(\lambda_1\cos\theta+\alpha\sin\theta)\frac{\partial\lambda_1}{\partial\tau}\right]d\tau + \int_{T_{H_0}}^{t}\frac{1}{\sqrt{t-\tau}}\,\mathrm{Im}\left[A_4(\lambda_2)K_{\mathrm{II}}^{\mathrm{F}}(\lambda_2\cos\theta+\beta\sin\theta)\frac{\partial\lambda_2}{\partial\tau}\right]H(br_0-\tau)\,d\tau + \int_{br_0}^{t}\frac{1}{\sqrt{t-\tau}}\,\mathrm{Im}\left[A_4(\lambda_3)K_{\mathrm{II}}^{\mathrm{F}}(\lambda_3\cos\theta+\beta\sin\theta)\frac{\partial\lambda_3}{\partial\tau}\right]d\tau, \tag{14}$$

where

$$\lambda_1 = \frac{\tau}{r_0}\cos\theta_0 + \mathrm{i}\sqrt{\frac{\tau^2}{r_0^2} - a^2}\sin\theta_0, \quad \lambda_2 = \frac{\tau}{r_0}\cos\theta_0 - \mathrm{sgn}\,(l)\sqrt{b^2 - \frac{\tau^2}{r_0^2}}\sin\theta_0,$$

$$\lambda_3 = \frac{\tau}{r_0}\cos\theta_0 + \mathrm{i}\sqrt{\frac{\tau^2}{r_0^2} - b^2}\sin\theta_0, \quad T_{H_0} = r_0(a|\cos\theta_0| + \sqrt{b^2-a^2}\sin\theta_0),$$

$$r_0^2 = l^2 + h^2, \quad \cos\theta_0 = \frac{l}{r_0}, \quad \sin\theta_0 = \frac{h}{r_0},$$

$$\mathrm{sgn}\,(l) = 1, \quad l > 0,$$

$$= -1, \quad l < 0. \tag{15}$$

The three terms in (13) and (14) represent the contribution of the primary wave (P wave), head wave (H wave), and shear wave (S wave), respectively. The H wave only exists in the region $|\cos\theta_0| > a/b$. Times equal to ar_0, T_{H_0} and br_0 represent arrival times of wave fronts of P, H and S waves, respectively. In the region $\cos\theta^* > a/b$, the branch point $\lambda_2 = -a\cos\theta - \sqrt{b^2-a^2}\sin\theta$ in the second term of (13) and (14) is embraced in the integral path. It represents the reflected head wave from the crack surface generated by the incident S wave, the corresponding arrival time of this wave front is $r_0(a\cos\theta^* + \sqrt{b^2-a^2}\sin\theta^*)$. The definition of θ^* is given in Fig. 1(a). If loading is applied at the right-hand side of the crack tip, the incident P, H and S waves reach the crack tip first and diffracted and reflected waves will be generated later. But if the loading is applied at the left-hand side, the incident P, H, and S waves reach the crack surface first, reflected waves from the crack surfaces arrive at the crack tip, and diffraction from the crack tip occurs.

Consider a more realistic impact loading for a uniformly distributed normal force from $\bar{x}_1 = l$ to l' with time dependence $H(t)$ as shown in Fig. 1(b). The stress intensity factors of this distributed loading can be obtained by taking integration of (11) and (12) in the Laplace transform domain:

$$\bar{K}_{\mathrm{I}} = \frac{1}{\sqrt{2\pi i p^{3/2}}}\int \frac{1}{\lambda} A_1(\lambda) K_{\mathrm{I}}^{\mathrm{F}}(\lambda\cos\theta + \alpha\sin\theta)(\mathrm{e}^{-p\alpha h - p\lambda l} - \mathrm{e}^{-p\alpha h - p\lambda l'})$$

$$+ \frac{1}{\lambda} A_2(\lambda) K_{\mathrm{I}}^{\mathrm{F}}(\lambda\cos\theta + \beta\sin\theta)(\mathrm{e}^{-p\beta h - p\lambda l} - \mathrm{e}^{-p\beta h - p\lambda l'})\,\mathrm{d}\lambda, \tag{16}$$

$$\bar{K}_{\mathrm{II}} = \frac{1}{\sqrt{2\pi i p^{3/2}}}\int \frac{1}{\lambda} A_3(\lambda) K_{\mathrm{II}}^{\mathrm{F}}(\lambda\cos\theta + \alpha\sin\theta)(\mathrm{e}^{-p\alpha h - p\lambda l} - \mathrm{e}^{-p\alpha h - p\lambda l'})$$

$$+ \frac{1}{\lambda} A_4(\lambda) K_{\mathrm{II}}^{\mathrm{F}}(\lambda\cos\theta + \beta\sin\theta)(\mathrm{e}^{-p\beta h - p\lambda l} - \mathrm{e}^{-p\beta h - p\lambda l'})\,\mathrm{d}\lambda. \tag{17}$$

To complete the solution, we must evaluate the integrals and invert the resulting expressions to the time domain. We shall accomplish this task by employing the Cagniard–de Hoop method. The contribution of pole at $\lambda = 0$ must be considered when deforming the integral path. If l and l' are less (or greater) than zero simultaneously, the Cauchy residual integral will be canceled out. So, the contribution of this pole only exists in the case of $l < 0$ and $l' > 0$. Because the values $A_2(0)$ and $A_4(0)$ are zero, the contribution of the pole of shear wave will vanish, and only the longitudinal wave exists. The final results for stress intensity factors in the time domain are

$$\frac{\pi^{3/2}}{2\sqrt{2}} K_{\mathrm{I}}(t) = \int_{ar_0}^{t} \sqrt{t-\tau}\,\mathrm{Im}\left[\frac{1}{\lambda_1} A_1(\lambda_1) K_{\mathrm{I}}^{\mathrm{F}}(\lambda_1\cos\theta + \alpha\sin\theta)\frac{\partial\lambda_1}{\partial\tau}\right]\mathrm{d}\tau$$

$$- \int_{ar_1}^{t} \sqrt{t-\tau}\,\mathrm{Im}\left[\frac{1}{\lambda_4} A_1(\lambda_4) K_{\mathrm{I}}^{\mathrm{F}}(\lambda_4\cos\theta + \alpha\sin\theta)\frac{\partial\lambda_4}{\partial\tau}\right]\mathrm{d}\tau$$

$$+\int_{T_{H_0}}^{t}\sqrt{t-\tau}\,\mathrm{Im}\left[\frac{1}{\lambda_2}A_2(\lambda_2)K_{\mathrm{I}}^{\mathrm{F}}(\lambda_2\cos\theta+\beta\sin\theta)\frac{\partial\lambda_2}{\partial\tau}\right]H(T_{\mathrm{S}}-\tau)\,\mathrm{d}\tau$$

$$-\int_{T_{H_1}}^{t}\sqrt{t-\tau}\,\mathrm{Im}\left[\frac{1}{\lambda_5}A_2(\lambda_5)K_{\mathrm{I}}^{\mathrm{F}}(\lambda_5\cos\theta+\beta\sin\theta)\frac{\partial\lambda_5}{\partial\tau}\right]H(T_{\mathrm{S}}-\tau)\,\mathrm{d}\tau$$

$$+\int_{br_0}^{t}\sqrt{t-\tau}\,\mathrm{Im}\left[\frac{1}{\lambda_3}A_2(\lambda_3)K_{\mathrm{I}}^{\mathrm{F}}(\lambda_3\cos\theta+\beta\sin\theta)\frac{\partial\lambda_3}{\partial\tau}\right]\mathrm{d}\tau$$

$$-\int_{br_1}^{t}\sqrt{t-\tau}\,\mathrm{Im}\left[\frac{1}{\lambda_6}A_2(\lambda_6)K_{\mathrm{I}}^{\mathrm{F}}(\lambda_6\cos\theta+\beta\sin\theta)\frac{\partial\lambda_6}{\partial\tau}\right]\mathrm{d}\tau$$

$$+\pi\sqrt{(t-ah)}A_1(0)K_{\mathrm{I}}^{\mathrm{F}}(a\sin\theta)H(t-ah), \tag{18}$$

$$\frac{\pi^{3/2}}{2\sqrt{2}}K_{\mathrm{II}}(t)=\int_{ar_0}^{t}\sqrt{t-\tau}\,\mathrm{Im}\left[\frac{1}{\lambda_1}A_3(\lambda_1)K_{\mathrm{II}}^{\mathrm{F}}(\lambda_1\cos\theta+\alpha\sin\theta)\frac{\partial\lambda_1}{\partial\tau}\right]\mathrm{d}\tau$$

$$-\int_{ar_1}^{t}\sqrt{t-\tau}\,\mathrm{Im}\left[\frac{1}{\lambda_4}A_3(\lambda_4)K_{\mathrm{II}}^{\mathrm{F}}(\lambda_4\cos\theta+\alpha\sin\theta)\frac{\partial\lambda_4}{\partial\tau}\right]\mathrm{d}\tau$$

$$+\int_{T_{H_0}}^{t}\sqrt{t-\tau}\,\mathrm{Im}\left[\frac{1}{\lambda_2}A_4(\lambda_2)K_{\mathrm{II}}^{\mathrm{F}}(\lambda_2\cos\theta+\beta\sin\theta)\frac{\partial\lambda_2}{\partial\tau}\right]H(T_{\mathrm{S}}-\tau)\,\mathrm{d}\tau$$

$$-\int_{T_{H_1}}^{t}\sqrt{t-\tau}\,\mathrm{Im}\left[\frac{1}{\lambda_5}A_4(\lambda_5)K_{\mathrm{II}}^{\mathrm{F}}(\lambda_5\cos\theta+\beta\sin\theta)\frac{\partial\lambda_5}{\partial\tau}\right]H(T_{\mathrm{S}}-\tau)\,\mathrm{d}\tau$$

$$+\int_{br_0}^{t}\sqrt{t-\tau}\,\mathrm{Im}\left[\frac{1}{\lambda_3}A_4(\lambda_3)K_{\mathrm{II}}^{\mathrm{F}}(\lambda_3\cos\theta+\beta\sin\theta)\frac{\partial\lambda_3}{\partial\tau}\right]\mathrm{d}\tau$$

$$-\int_{br_1}^{t}\sqrt{t-\tau}\,\mathrm{Im}\left[\frac{1}{\lambda_6}A_4(\lambda_6)K_{\mathrm{II}}^{\mathrm{F}}(\lambda_6\cos\theta+\beta\sin\theta)\frac{\partial\lambda_6}{\partial\tau}\right]\mathrm{d}\tau$$

$$+\pi\sqrt{(t-ah)}A_3(0)K_{\mathrm{II}}^{\mathrm{F}}(a\sin\theta)H(t-ah), \tag{19}$$

where

$$\lambda_4=\frac{\tau}{r_1}\cos\theta_1+\mathrm{i}\sqrt{\frac{\tau^2}{r_1^2}-a^2}\sin\theta_1,\quad \lambda_5=\frac{\tau}{r_1}\cos\theta_1-\mathrm{sgn}\,(l')\sqrt{b^2-\frac{\tau^2}{r_1^2}}\sin\theta_1,$$

$$\lambda_6=\frac{\tau}{r_1}\cos\theta_1+\mathrm{i}\sqrt{\frac{\tau^2}{r_1^2}-b^2}\sin\theta_1,\quad T_{H_1}=r_1\left(a|\cos\theta_1|+\sqrt{b^2-a^2}\sin\theta_1\right),$$

$$r_1^2=l'^2+h^2,\quad \cos\theta_1=\frac{l'}{r_1},\quad \sin\theta_1=\frac{h}{r_1},$$

$$\mathrm{sgn}\,(l')=1,\qquad l'>0,$$

$$=-1,\quad l'<0. \tag{20}$$

The last term of both (18) and (19) represents the effect of the straight plane wave emitted from the surface l to l'. The resulting wave pattern for the uniformly distributed impact loading is shown in Fig. 1(b). The last terms in both (18) and (19) are due to the downward plane wave while the remaining six integrals are related to the two edge effects of the loading interval on the surface. Equations (18) and (19) are valid only if the crack tip is under the loaded region. The respective arrival times of the wave fronts are ar_0, T_{H_0} and br_0 for the P, H and S waves in the left-hand side, and ar_1, T_{H_1} and br_1 for the same waves in the right-hand side. Finally, ah is the arrival time of the straight P wave. The head wave exists only

in the regions $|\cos\theta_0| > a/b$ and $|\cos\theta_1| > a/b$, while the straight P wave occurs in the infinite strip from l to l'.

In realistic impact loading conditions, it is impossible to produce a true loading of Heaviside function time dependence. Instead, the loading pulse has a finite rise time. Therefore, to simulate the practical impact event, the analysis is extended to a case where the loading pulse has a finite rise time. Suppose that at time $t = 0$, the pulse is applied suddenly and the magnitude of the pressure increases according to the function $f(t)$ as

$$f(t) = \frac{t}{T_R} \quad \text{for} \quad 0 \leqslant t \leqslant T_R,$$
$$= 1 \quad \text{for} \quad T_R < t, \tag{21}$$

where T_R is the rise time. Then, the stress intensity factors can be obtained by the superposition method

$$K'_{I,II}(t) = \int_0^t \frac{df(\tau)}{d\tau} K_{I,II}(t-\tau)\, d\tau, \tag{22}$$

where $K_{I,II}(t)$ are the stress intensity factors for a unit step stress wave loading profile as presented in (18) and (19).

Practical structures are not only subjected to tension but also to shear loading. In mixed mode experiments, it is usually observed that crack extension takes place at an angle with respect to the original crack. When the mixed stress intensity factors have been obtained, the criteria of maximum circumferential tensile stress proposed by Erdogan and Sih (1963) and minimum strain energy density proposed by Sih (1972) will be introduced to examine the crack growth direction. The maximum circumferential tensile stress criterion postulates that the crack will grow in a direction determined by the condition that when the circumferential tensile stress within the asymptotic field is at a maximum, the angle θ_2 $(= \theta - \theta_c)$ between the crack line and the direction of crack growth satisfies

$$\sin\theta_2 K_I + (3\cos\theta_2 - 1)K_{II} = 0. \tag{23}$$

The strain energy density criterion states that crack growth takes place in the direction of minimum strain energy density. The relation for determining θ_2, the angle of crack extension, is then given by

$$(1-2\nu)(-2\sin\theta_2 K_I^2 - 4\cos\theta_2 K_I K_{II} + 2\sin\theta_2 K_{II}^2)$$
$$+ (\sin 2\theta_2 K_I^2 + 4\cos 2\theta_2 K_I K_{II} - 3\sin 2\theta_2 K_{II}^2) = 0. \tag{24}$$

4. NUMERICAL RESULTS

In the previous sections, the exact elastodynamic stress intensity factor history has been determined. For numerical calculation of the mixed dynamic stress intensity factors, Poisson's ratio ν is assumed to be equal to 0.25. In this case, the ratios of the slownesses are $b = \sqrt{3}a$ and $c = 1.88a$. The point impact loadings of Heaviside function $H(t)$ time dependence are applied at the positions $l = -2h, 0$ and $2h$. The inclined angles θ of crack are 0°, 45° and 90°. There are nine combinations of loading position and inclined crack angle. The dynamic stress intensity factors for the time interval of interest are shown in

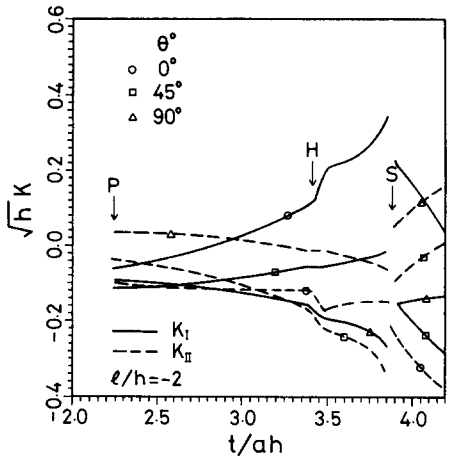

Fig. 2. Stress intensity factors K_I and K_{II} for point impact loading at $l = -2h$.

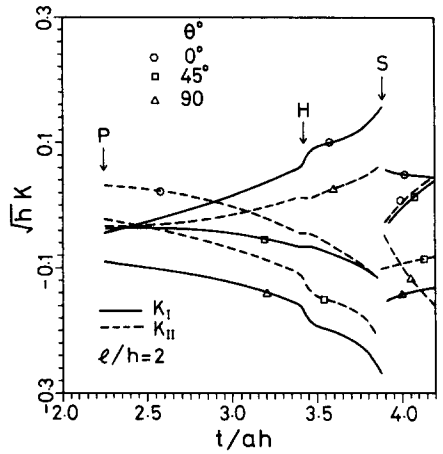

Fig. 3. Stress intensity factors K_I and K_{II} for point impact loading at $l = 2h$.

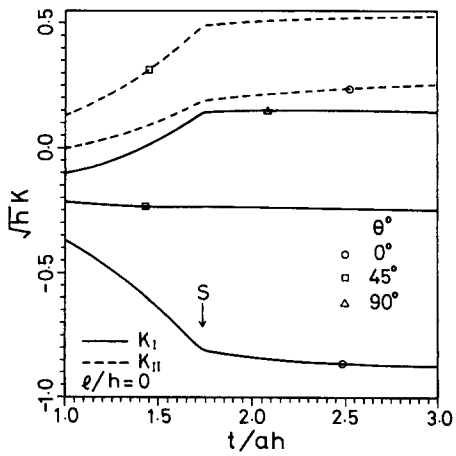

Fig. 4. Stress intensity factors K_I and K_{II} for point impact loading at $l = 0$.

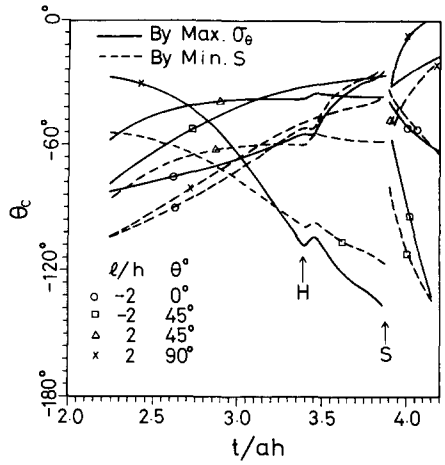

Fig. 5. Prediction of crack propagation direction for point loading.

Figs 2–4. The crack propagation angle θ_c that satisfies (23) and (24) for the problem analysed here is shown in Figs 5 and 6.

We consider first the case of an applied loading at the left (right)-hand side of the crack tip which makes $l = -2h$ ($l = 2h$). As indicated previously, the results obtained in this study are valid for the time period in which waves generated at the impact point and its diffractions from the notch end have not yet returned to the crack tip, that is $\sqrt{5} \leqslant t/ah \leqslant \sqrt{5}+2$. There are incident P, H and S waves from the applied loading point on the semi-infinite surface. The normalized arrival times t/ah of incident wave fronts at the crack tip are $\sqrt{5}$ for the P wave, $2+\sqrt{2}$ for the H wave, and $\sqrt{15}$ for the S wave. The exact stress intensity factors are given in Figs 2 and 3. For the case of $l/h = -2$ and $\theta = 0°$ as shown in Fig. 2, although the reflected wave generated from the crack surface begin to reach the crack tip at time $t/ah = \sqrt{13} = 3.6$ after being reflected from the half space free boundary, the stress intensity factor evaluated for this case does not account for the contribution of this reflected wave from the free boundary. The histories of stress intensity factors have a finite jump at P and S wave fronts. It is shown that the arrival of the longitudinal wave instantaneously places the crack edge is compression. For $\theta = 0$, Figs 2 and 3 show that the crack tip stress field changes from compression to tension, and the tension field grows subsequently prior to the shear wave arrival. If θ is equal to 45° or 90°, the transient field near the crack tip is in compression during the whole time interval of

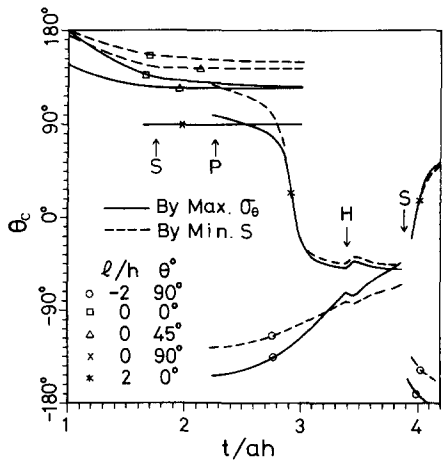

Fig. 6. Prediction of crack propagation direction for point loading.

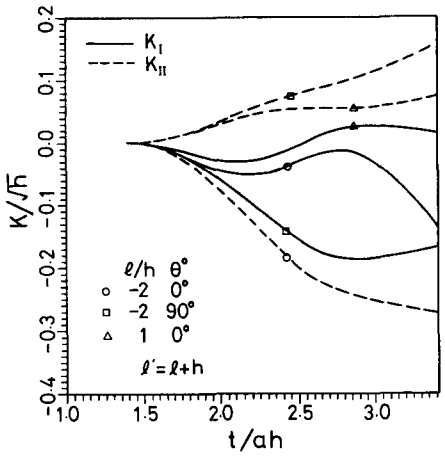

Fig. 7. Stress intensity factors K_I and K_{II} for uniformly distributed loading.

interest. If loading is applied at $l = 0$, the case in which a normal point force is applied directly above the crack tip, only P and S waves pass through the crack tip. As shown in Fig. 4, a finite value is found at the longitudinal wave front but no jump occurs at the shear wave front. The valid time interval in this case is $1 \leqslant t/ah \leqslant 3$. The normalized arrival times are 1 for the P wave and $\sqrt{3}$ for the S wave. If $\theta = 90°$, the crack is perpendicular to the half-plane surface, we have the case studied by Brock *et al.* (1985). We can see from Figs 2–4 that if one wants to design an impact loading system which will result in a positive mode I stress intensity factor, the most suitable arrangement will be to put the crack parallel to the free surface and to have the dynamic impact loading applied at the free boundary at the position above the crack surface, as indicated in Fig. 2 for the case of $\theta = 0°$.

Without considering the feasibility when the compression state is generated in the near tip, the crack propagation angle θ_c predicted by maximum circumferential tensile stress and minimum strain energy density criteria for the problem analysed here is shown in Figs 5 and 6. It can be concluded from these two figures that the most dangerous case will be one of a loading applied directly above the crack tip (i.e. $l = 0$) because, in this case, the crack propagation angle θ_c is always greater than zero, meaning that the crack will propagate toward the half-plane surface.

In order to simulate a realistic situation with practical applications, we consider the uniformly distributed impact loading shown in Fig. 1(b). There are three kinds of loading position to be investigated numerically. They are a distributed loading applied at the left-hand side of the crack tip ($l = -2h$, $l' = -h$), a distributed loading applied symmetrically with respect to the crack tip ($l = -0.5h$, $l' = 0.5h$), and a distributed loading applied at the right-hand side of the crack tip ($l = h$, $l' = 2h$). The orientation of the crack can be parallel or perpendicular to the half-plane surface. The time dependent loading impulse has a finite rise time as indicated in (21). A normalized rise time T_R equal to $0.5ah$ is chosen for the numerical study. The dynamic stress intensity factors have been evaluated numerically and are shown in Figs 7 and 8. The result shows a continuation of the stress intensity factor at the wave front, which differs from the case of an applied point loading with Heaviside function time dependence discussed previously. The maximum circumferential tensile stress criterion is used for prediction of the crack propagation direction for the distributed loading condition the result of which is shown in Fig. 9. It is noted that if the distributed loading is applied directly above the crack tip, the crack will propagate toward the half-plane surface. For a horizontal crack subjected to a distributed loading located on the right-hand side of the crack tip, the crack will also tend to propagate toward the half-plane surface.

5. CONCLUSIONS

In this study, an exponentially distributed loading on the crack surfaces in the Laplace transform domain is considered as the fundamental solution. The incident waves from

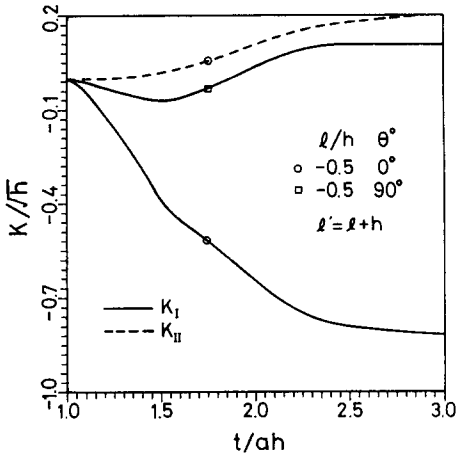

Fig. 8. Stress intensity factors K_I and K_{II} for uniformly distributed loading.

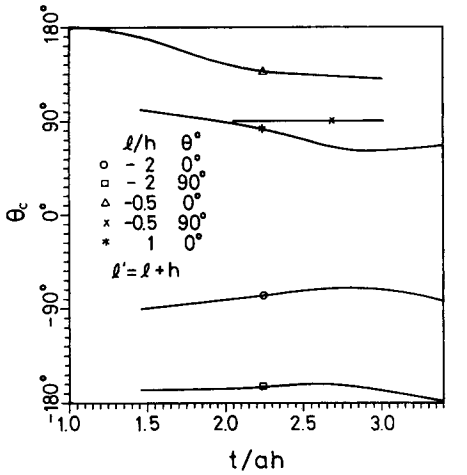

Fig. 9. Prediction of crack propagation direction subjected to uniformly distributed loading.

the impact loading diffracted by the crack tip can be constructed by superimposing the fundamental solution. This new methodology is shown to be both powerful and efficient in solving more complex and difficult problems.

In the previous sections, a subsurface inclined crack subjected to impact loading on a half-plane surface is investigated. The net result of this loading will induce a mixed mode field at the crack tip. Exact mixed mode I and II stress intensity factors are obtained in an explicit form. The exact solution to this configuration can provide a valuable check for pure numerical methods such as the finite element, finite difference or boundary element methods in solving more complex geometries.

The maximum circumferential tensile stress and minimum strain energy criteria are used to predict the direction of crack propagation. It is found in this study that the crack will extrude out of the half-plane surface if the impact loading is applied in the region above the crack tip.

Acknowledgement—The work described here was supported by the National Science Council (Republic of China), through grant NSC 79-0401-E-002-36 to National Taiwan University. This research support is gratefully acknowledged.

REFERENCES

Brock, L. M. (1982). Shear and normal impact loadings on one face of a narrow slit. *Int. J. Solids Structures* **18**, 467–477.

Brock, L. M. (1984). Stresses in a surface obstacle undercut due to rapid indentation. *J. Elasticity* **14,** 415–424.
Brock, L. M., Jolles, M. and Schroedl, M. (1985). Dynamic impact over a subsurface crack : Applications to the dynamic tear test. *J. Appl. Mech.* **52,** 287–290.
Erdogan, F. and Sih, G. C. (1963). On the crack extension in plates under plane loading and transverse shear. *J. Basic Engng* **85,** 519–527.
Freund, L. B. (1974). The stress intensity factor due to normal impact loading of the faces of a crack. *Int. J. Engng Sci.* **12,** 179–189.
de Hoop, A. T. (1958). Representation theorems for the displacement in an elastic solid and their application to elastodynamic diffraction theory. Doctoral Dissertation, Technische Hoegschool, Delft.
Lamb, H. (1904). On the propagation of tremors over the surface of an elastic solid. *Phil. Trans. Roy. Soc. Lond.* **A203,** 1–42.
Lee, Y. J. and Freund, L. B. (1990). Fracture initiation due to asymmetric impact loading of an edge cracked plate. *J. Appl. Mech.* **57,** 104–111.
Ma, C. C. and Hou, Y. C. (1990). Theoretical analysis of the transient response for a stationary inplane crack subjected to dynamic impact loading. *Int. J. Engng Sci.* **28,** 1321–1329.
Ma, C. C. and Hou, Y. C. (1991). Transient analysis for antiplane crack subjected to dynamic loadings. *J. Appl. Mech.* **58,** 703–709.
Noble, B. (1958). *The Wiener–Hopf Technique*. Pergamon Press, Oxford.
Sih, G. C. (1972). Strain energy density factor applied to mixed mode crack problems. Institute of Fracture and Slolid Mechanics. Technical Report, Lehigh University.
Tsai, C. H. and Ma, C. C. (1992). Transient analysis of a semi-infinite crack subjected to dynamic concentrated forces. *J. Appl. Mech.* **59,** 804–811.